$K\alpha_{1,2}$ x-ray linewidths, asymmetry indices, and $[KM]$ shake probabilities in elements Ca to Ge and comparison with theory for Ca, Ti, and Ge

Y. Ito,[1] T. Tochio,[2] H. Ohashi,[3] M. Yamashita,[4] S. Fukushima,[5] M. Polasik,[6] K. Słabkowska,[6] Ł. Syrocki,[7] E. Szymańska,[6] J. Rzadkiewicz,[8] P. Indelicato,[9] J. P. Marques,[10,11] M. C. Martins,[11] J. P. Santos,[11] and F. Parente[10,11,*]

[1]*ICR, Kyoto University, Gokasho, Uji, Kyoto 611-0011, Japan*

[2]*Faculty of Science, Kobe University, 1-1 Rokkodai, Kobe 657-8501, Japan*

[3]*Accuray Japan K. K., 2-2-1 Ootemachi, Chiyoda-ku, Tokyo 100-0004, Japan*

[4]*HIT, 3-1-12 Yukihira, Suma-ku, Kobe 654-0037, Japan*

[5]*NIMS, 1-2-1 Sengen, Tsukuba, Ibaraki 305-0047, Japan*

[6]*Faculty of Chemistry, Nicolaus Copernicus University in Toruń, Gagarina 7, 87-100 Toruń, Poland*

[7]*Faculty of Physics, Astronomy and Informatics, Nicolaus Copernicus University in Toruń, Grudziadzka 5, 87-100 Toruń, Poland*

[8]*National Centre for Nuclear Studies, 01-497 Warsaw, Poland*

[9]*Laboratoire Kastler Brossel, UPMC-Sorbonne Universités, CNRS, ENS-PSL Research University, Collège de France, Case 74; 4, place Jussieu, F-75005 Paris, France*

[10]*BioISIBiosystems and Integrative Sciences Institute, Faculdade de Ciências da Universidade de Lisboa, Campo Grande, C8, 1749-016 Lisboa, Portugal*

[11]*Laboratório de Instrumentação, Engenharia Biomédica e Física da Radiação (LIBPhys-UNL), Departamento de Física, Faculdade de Ciências e Tecnologia da Universidade Nova de Lisboa, Monte da Caparica, 2892-516 Caparica, Portugal*

(Received 27 May 2016; published 6 October 2016)

We have investigated systematically the $K\alpha$ x-ray spectra in elements from Ca to Ge within Berger's two-Lorentzian functions model, using a high-resolution antiparallel double-crystal x-ray spectrometer, in order to obtain in detail the physical meaning of the asymmetry in the spectral profiles. The overall tendency of the corrected full width at half maximum of the $K\alpha_1$ and $K\alpha_2$ lines as a function of Z, as well as the linewidths, are in good agreement with the data reported in the literature. It is found, from both the experiments and calculation, that satellite lines arising from shake-off appear between the $K\alpha_1$ and $K\alpha_2$ lines. The asymmetry index of $K\alpha_1$ in $3d$ elements from Sc to Zn is ascribed to the existence of a $3d$ spectator hole. Moreover, the observed Sc $K\alpha_1$ line shows a symmetric profile unlike the Ti $K\alpha_1$ line profile, this discrepancy being explained by the existence of satellite lines on both sides of the Sc profile. Our experimental results yielded around 25% probability for the probability of shake processes creating a second hole in the $3p$ or $3d$ subshells in Sc and around 18% probability for creating a second hole the in the $3p$ in Ca. For the latter process our calculated value, using multiconfiguration Dirac-Fock wave functions and the sudden approximation yielded a 10% probability.

DOI: 10.1103/PhysRevA.94.042506

I. INTRODUCTION

Research on the width and shape of the asymmetric $K\alpha$ x-ray doublet of $3d$ elements ($21 \leqslant Z \leqslant 30$) has been the object of interest for a long time, both from the theoretical and experimental points of view [1]. Although several causes have been proposed to explain this asymmetry such as, for example, shake processes [2], conduction-band collective excitations [3], exchange [4], and final-state interactions [5], the origin of the asymmetric shape is still under investigation and debate [6–8].

In order to obtain a simple description of the Cu $K\alpha_{1,2}$ spectrum, Berger [9] assumed a doublet model for each of the $K\alpha_1$ and $K\alpha_2$ peaks and used two pairs of Lorentzian functions, denominated $K\alpha_{11}$ and $K\alpha_{12}$, and $K\alpha_{21}$ and $K\alpha_{22}$, respectively, to fit them. A physical meaning for this simple model was given by Deutsch *et al.* [6], based on the theoretical reasoning that the asymmetry in Cu $K\alpha$ spectra is due to the existence of shake processes leading to a $3d$ spectator hole. When a hole is created in the $1s$ shell, there is a probability that a second hole is created also in the $3d$ subshell. This shake-off process leaves the system with two holes and will be referred to subsequently as $[1s3d]$ shake (or $[KM]$ if the second hole is created in any of the M subshells). Thus, the $K\alpha_{11}$ and $K\alpha_{21}$ Lorentzian peaks would correspond to the $K\alpha_1$ and $K\alpha_2$ diagram lines, respectively, and the $K\alpha_{21}$ and $K\alpha_{22}$ peaks to the corresponding satellite lines.

In a similar way, Ito *et al.* [10,11] attributed the asymmetry in Zn $K\alpha_{1,2}$ spectra to the $[1s3d]$ shake processes. Using the two-Lorentzian model, Ito *et al.* [11] and Polasik *et al.* [12] investigated the emission line shape in elements Ti to Zn and concluded that the full width at half maximum (FWHM) of the $K\alpha_{11}$ line is higher in these elements than the theoretical values reported by Krause and Oliver [13].

Moreover, Ito *et al.* [11] reported that the behavior of the variation with Z of the $K\alpha_{21}$ line FWHM is different from that of the variation of the $K\alpha_{11}$ line FWHM, this being ascribed to the satellite lines resulting from the L_2-$L_3M_{4,5}$ Coster-Kronig transitions. On the other hand, Hölzer *et al.* [7] analyzed these lines with a single-crystal spectrometer, using a number of Lorentzian functions that varied from two in Ni and Cu, to four in Fe and Co, and five in Cr and Mn, respectively. Recently, Chantler *et al.* [8] reanalyzed $K\alpha$ spectra from Sc to Mn,

*Corresponding author: facp@fct.unl.pt

already published by other authors, with the single exception of V whose spectra were obtained by themselves. Again, several Lorentzian functions were employed to fit the experimental data.

The satellite lines that explain the asymmetry of $K\alpha$ lines are originated mostly by shake-off processes. Anagnostopoulos *et al.* [14] obtained for the $[1s3p]$ and $[1s3d]$ shake probabilities in Sc 15% and 38%, respectively. The latter value agrees with the 40% value estimated by Lowe *et al.* [15].

As has been emphasized recently by Chantler *et al.* [16], experimentally reported linewidths in the transition metals are in many cases discrepant by 1 eV or more, such as the widely measured Cu $K\alpha_2$ width which ranges from 2.89 to 4.05 eV. Thus, a long-term controversy still continues about the origin of the asymmetries affecting the $K\alpha$ x-ray lines of the $3d$ elements. Also, a broad symmetric instrumental function generally tends to suppress the line asymmetry and yields systematically smaller values for the asymmetry index, defined as the ratio of the half widths at half height on the low and high energy sides of the peak. For instance, in the Cu $K\alpha_1$ emission spectrum, the width of the instrumental function in our antiparallel setting was $\Delta E \sim 0.15$ eV for the Si(220) crystal and $\Delta E \sim 1.19$ eV for the Ge(111) crystal, ten times larger than the former.

As it was considered that a simple description of the peak profiles by two Lorentzian functions was acceptable for the Cu $K\alpha$ lines, in the present work we analyzed systematically the $K\alpha$ emission spectra in elements from Ca to Ge using the same model, in order to elucidate the physical meaning of the asymmetry index of the lines, and the contribution of the $[KM]$ shake processes. We also investigated the contribution of the primary targets (Rh and W) to the linewidths and the shake processes. Moreover, we examined from the theoretical point of view the shake processes in Ca, Ti, and Ge, together with their spectral profiles. Our aim is to obtain systematic atomic information on the $K\alpha$ spectra of the $3d$ elements, using a high-resolution double-crystal x-ray spectrometer.

II. EXPERIMENTAL METHODOLOGY

The fluorescent $K\alpha$ x-ray spectra of elements Ca to Ge were measured using a Rigaku double-crystal spectrometer (System 3580EKI) shown schematically in Fig. 1. Similarly to the single-crystal Johann type x-ray spectrometer, the instrumental function consists in the convolution of the crystal rocking curves with the slit function of a Soller slit in the system. Its resolution depends only on the crystals faultlessness. The second crystal plays an important role as a shutter, intersecting the extra rays that do not satisfy Bragg's law on the first crystal. Or, alternatively, the first crystal works as a slit before the second crystal. The (+,+) configuration (antiparallel) double convolution process of the two instrumental functions results in an effective high resolution. In the case of a double-crystal spectrometer with higher order Bragg reflections, it was possible to make the instrumental function so narrow that a correction for window function is negligible (see Tochio *et al.* [17] for details). For this reason, in the present work we used a double-crystal spectrometer system. An end-window type was adopted as the primary x-ray source without the contamination of the filament material, usually, tungsten.

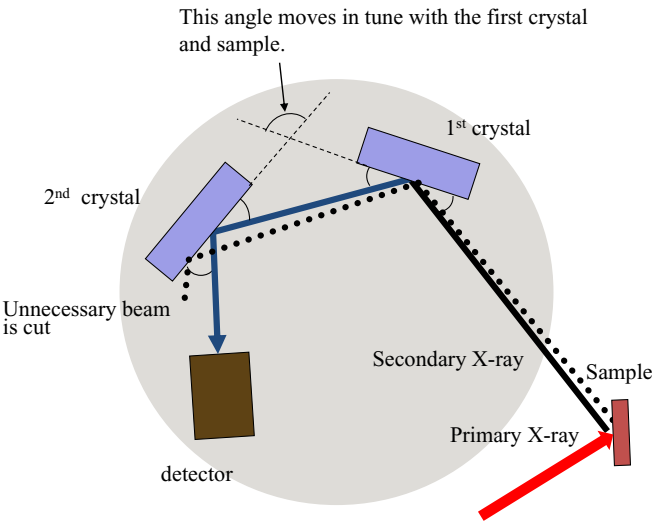

FIG. 1. The double flat crystal x-ray spectrometer used in this work. The first and second crystals are located in the (+,+) configuration with the detector. Upon being bombarded by a primary x-ray beam, secondary x rays are emitted from a sample. The secondary x rays are diagram lines characteristic of the constituent elements of the sample. The angle (marked by an arrow) made from the first and the second crystals moves in tune with the first crystal and the sample. Unnecessary x rays (marked by a broken line) are discarded at the second crystal due to being out of Bragg angle. The most suitable crystals should be selected for the samples.

Experimental conditions are listed in Table I. The observed $K\alpha_{1,2}$ emission spectra for elements Ca to Ge are shown in Figs. 2 and 3. The symmetric Si (220), Si(111), Si(400), Ge(111), and Ge(333) reflections were used in both crystals. As targets, we used CaF_2 crystal powder for Ca, foils for Sc, V, Co, and Ni, and plates for Ti, Mn, Fe, Cu, Zn, and Ge, respectively. The load of the primary x-ray tube was generally 40 kV, and 60 or 70 mA. The spectra were measured using an $Ar_{0.9}$ $(CH4)_{0.1}$ gas flow or a sealed Xe gas proportional counter. The latter has a good efficiency for high energy. The available 2θ angles are in the 20°–147° range. Temperature in the x-ray spectrometer chamber is controlled within 35.0 ± 0.5 °C. Neither smoothing nor correction were applied to the raw data. For the energy calibration the values of Bearden [18] were used as references for diagram lines. The spectrometer vertical divergence slit is 0.573°.

III. THEORETICAL METHODS

A. Relativistic calculations

Theoretical predictions of the shape of $K\alpha_{1,2}$ diagram and satellite lines have been performed using the multiconfiguration Dirac-Fock (MCDF) method [19–30]. For the description of the specific codes and further details, we refer the reader to Refs. [19,22,27–29]. The MCDF approach has the merit of including a large amount of electronic correlation with a small number of configurations [24,25,31–33].

Nuclear size effects were taken into account by using a uniformly charged sphere, and the atomic masses and the nuclear radii were taken from the tables by Audi *et al.* [34] and Angeli [35], respectively. Radiative corrections are also

TABLE I. Experimental conditions of the measurements using a two-crystal x-ray spectrometer. The measurements were done with a tube voltage of 40 kV and in vacuum, except the one referred to as "Si(220) air".

Z	Samples	Analyzing Crystal	Accumulation time (s/point)	Step [degree (2θ)]	Target element for excitation	Current (mA)	Number of measuring times
20	CaF_2 pellet	Si(220)	8	0.0005	Rh	60	3
21	Metal foil	Si(220)	20, 500	0.0005, 0.001. 0.002	Rh	60, 70	5
22	Metal plate	Si(220)	20	0.0005	W	70	8
		Si(220)	15	0.0005	Rh	60	3
23	Metal foil	Si(220)	15, 300	0.001	W	60, 70	6
24	Metal plate	Si(220)	15, 25	0.001, 0.0005	W	60, 70	4
		Si(220)	10, 30	0.0005	Rh	70	4
25	Metal plate	Si(220)	20	0.001	W	70	12
		Si(220)	30, 60	0.001, 0.0005	Rh	60	9
26	Metal plate	Si(220)	10	0.001	W	60	10
		Si(220)	30	0.001, 0.0005	Rh	60	12
		Ge(333)	20	0.005, 0.002	W	60	19
27	Metal foil	Si(220)	10	0.0005	W	70	5
		Si(220)	10	0.001	Rh	70	5
28	Metal foil	Si(220)	20	0.001, 0.0005	Rh	60	8
29	Metal plate	Si(220) air	5, 10, 50	0.001, 0.0005	W	70	12
		Si(220)	5	0.001	W	70	4
		Si(220)	10, 20	0.0005	Rh	60, 70	4
		Si(400)	5, 10, 60	0.001, 0.0005	W	70	3
		Si(220)	50	0.0005	Rh	70	3
		Ge(333)	60	0.001	W	60	5
		Si(440)	100	0.001	W	70	1
30	Metal foil	Si(220)	2, 20	0.0005	W	70	3
		Si(220)	20	0.0005	Rh	70	3
32	Metal plate	Si(220)	7	0.0005	Rh	60	3

introduced from a quantum electrodynamics (QED) treatment. The one-electron self-energy is evaluated using the one-electron values of Mohr and co-workers [36–39] and corrected for finite nuclear size [40]. The self-energy screening and vacuum polarization were included considering the methods developed by Indelicato and co-workers [21,26,39,41,42].

The code was used in the single-configuration approach, with the Breit interaction and the vacuum polarization terms included in the self-consistent field process, and other QED effects included as perturbations. For the determination of the transition rate and energy values we calculated independently the initial and final state wave functions in the so-called optimized level scheme, and the formalism proposed by Löwdin [43] to treat the nonorthogonality effects was employed. Further details can be found in Ref. [44]. The length gauge was used for all radiative transition probabilities.

The transition energy accuracy of the calculations using this method were studied by Indelicato and co-workers [41] who found very good agreement with experiments, later confirmed by Deslattes *et al.* [45].

Our present computations seem to be slightly better than those in [45]. Therefore, we can expect that the precision of our simulations for the satellite line shapes and positions is much more accurate. In particular, the energy shifts for studied $3d$-transition metals is much more accurate, i.e., in the order of 0.01–0.05 eV.

In what concerns transition rate uncertainties, they depend on the atomic number and on the considered particular shell, being higher for low Z atoms and for higher shells. We estimated the uncertainty in the transition rates from the relative difference between the values obtained in the length and velocity gauges. These are of the order of 3% for the dominant K-shell transitions.

B. Shake-off

A fast removal of an innermost electron causes a sudden change in the atomic potential, which may originate an atomic electron excitation to a higher shell (shake-up) or to the continuum (shake-off). In the incident-particle (photons or electrons) high-energy limit, one may use the so-called sudden approximation [46], in which the atomic excitation is treated separately from the initial vacancy creation process. Experimental results of Carlson [47] and Carlson *et al.* [48], as well as theoretical predictions of Krause and Carlson [49], Sachenko and Burtsev [50], Santos *et al.* [51], and Mauron *et al.* [52], support the validity of this approximation for atomic excitation following inner-shell vacancy production.

Within the sudden-approximation framework, the shake-off plus shake-up probability for removing one or more electrons from an orbital $|\psi_{n\ell j}\rangle$, where n and ℓ are the principal and orbital angular-momentum quantum numbers and $j = \ell \pm \frac{1}{2}$, when a hole is created in shell or subshell $n'l'j'$, is given by

$$Q_{n'l'j'}(n\ell j) = 1 - (|\langle\psi_{n\ell j}(A^+)|\psi_{n\ell j}(A)\rangle|^2)^N - P_{\rm F}, \quad (1)$$

where $|\psi_{n\ell j}(A)\rangle$ represents the orbital $n\ell j$ of the neutral atom and $|\psi_{n\ell j}(A^+)\rangle$ represents the orbital $n\ell j$ in the ion A^+

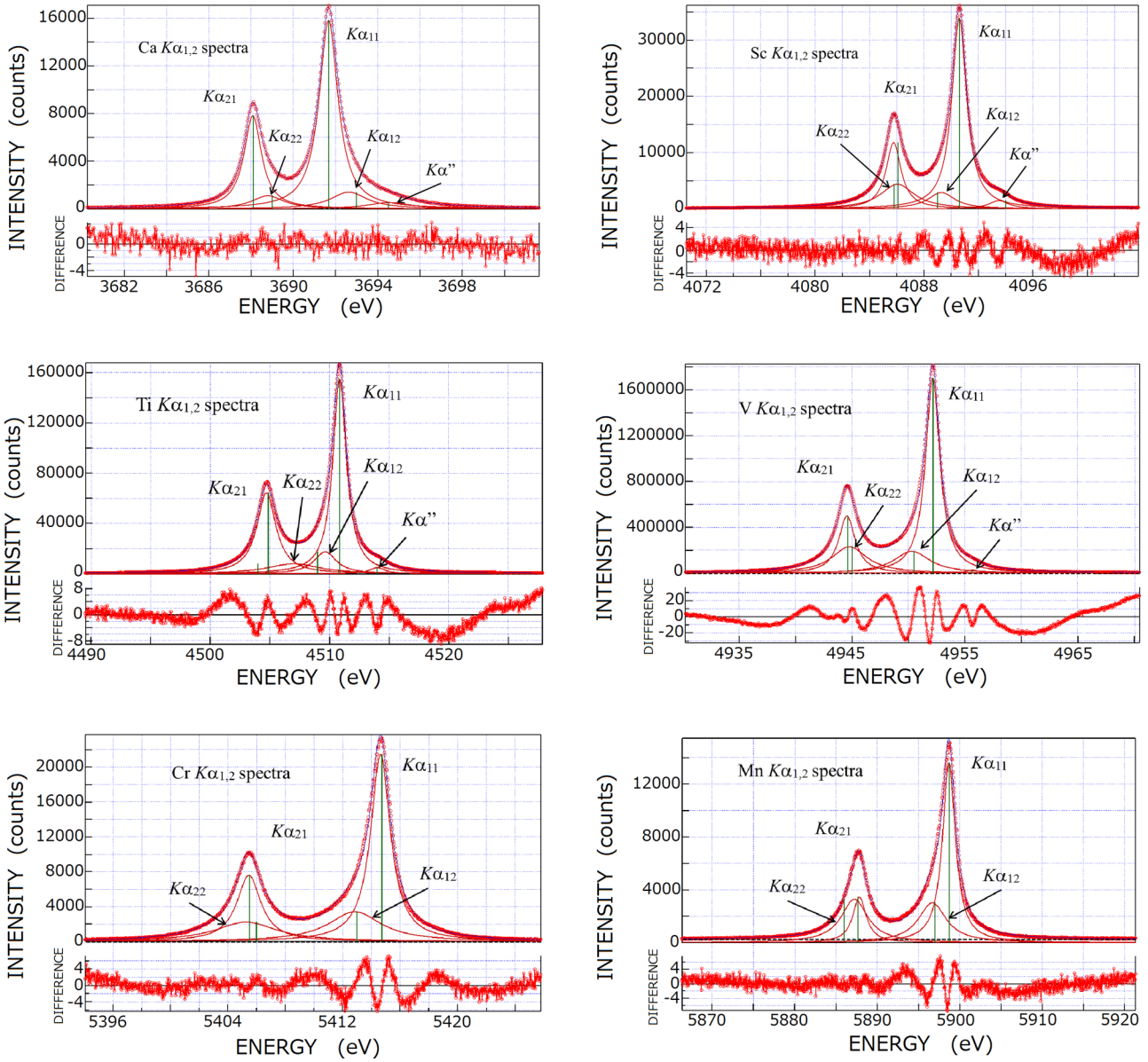

FIG. 2. The observed $K\alpha_{1,2}$ spectra in elements Ca to Mn are shown with the Lorentzian functions used in the fitting process [6,9,11]. These spectra were measured using the antiparallel double-crystal x-ray spectrometer described in the text. $K\alpha_{11}$ is the $K\alpha_1$ diagram line, and $K\alpha_{21}$ is the $K\alpha_2$ line. $K\alpha_{12}$ and $K\alpha_{22}$ satellite lines are due to $2p \rightarrow 1s$ electron transitions in the presence of an extra $3d$ hole resulting from shake processes. The $K\alpha''$ line is a satellite line ascribed to a $3p$ spectator hole.

whereby a single vacancy has been created in a subshell $n'l'j'$ of atom A. N is the number of electrons in orbital $n\ell j$.

The quantity $P_{\rm F}$ is a correction which arises from the condition that electron shake-up transitions to occupied levels are not physically allowed. The corrections for contributions to filled states (from $n' = 1$ to x) is

$$P_{\rm F} = \sum_{n'=1}^{n'=x} \frac{NN'}{2j+1} |\langle \psi_{n'\ell j}(A^+) | \psi_{n\ell j}(A) \rangle|^2, \qquad (2)$$

where $n' \neq n$, and N' is the number of electrons in the orbital designated by $n'\ell j$.

In this work, the electron shake-off plus shake-up probabilities as the result of single K-shell ionization have been calculated in the sudden approximation model, Eq. (1), using the multiconfiguration Dirac-Fock wave functions [53] for the neutral atom (initial state) and for the ion with a single $1s$ hole (final state), for selected atoms with $20 \leqslant Z \leqslant 32$. Moreover, we compared the observed of $K\alpha_{1,2}$ spectra in Ca ($3d^0$), Ti ($3d^2$), and Ge ($3d^{10}$) elements with theoretical calculations based on the shake processes.

In order to obtain the satellite line intensity $I_{\rm S}(K\alpha_{1,2})$ in Ti, Ca, and Ge (when a hole is created in the K subshell) we needed to calculate the shake-off plus shake-up probabilities for production of $[1s3d]$ and $[1s3p]$ for Ti, $[1s3p]$, $[1s3s]$, and $[1s4s]$ for Ca, and $[1s3d]$, $[1s3p]$, $[1s3s]$, $[1s4p]$, and $[1s4s]$ for Ge hole states, respectively (see Fig. 6).

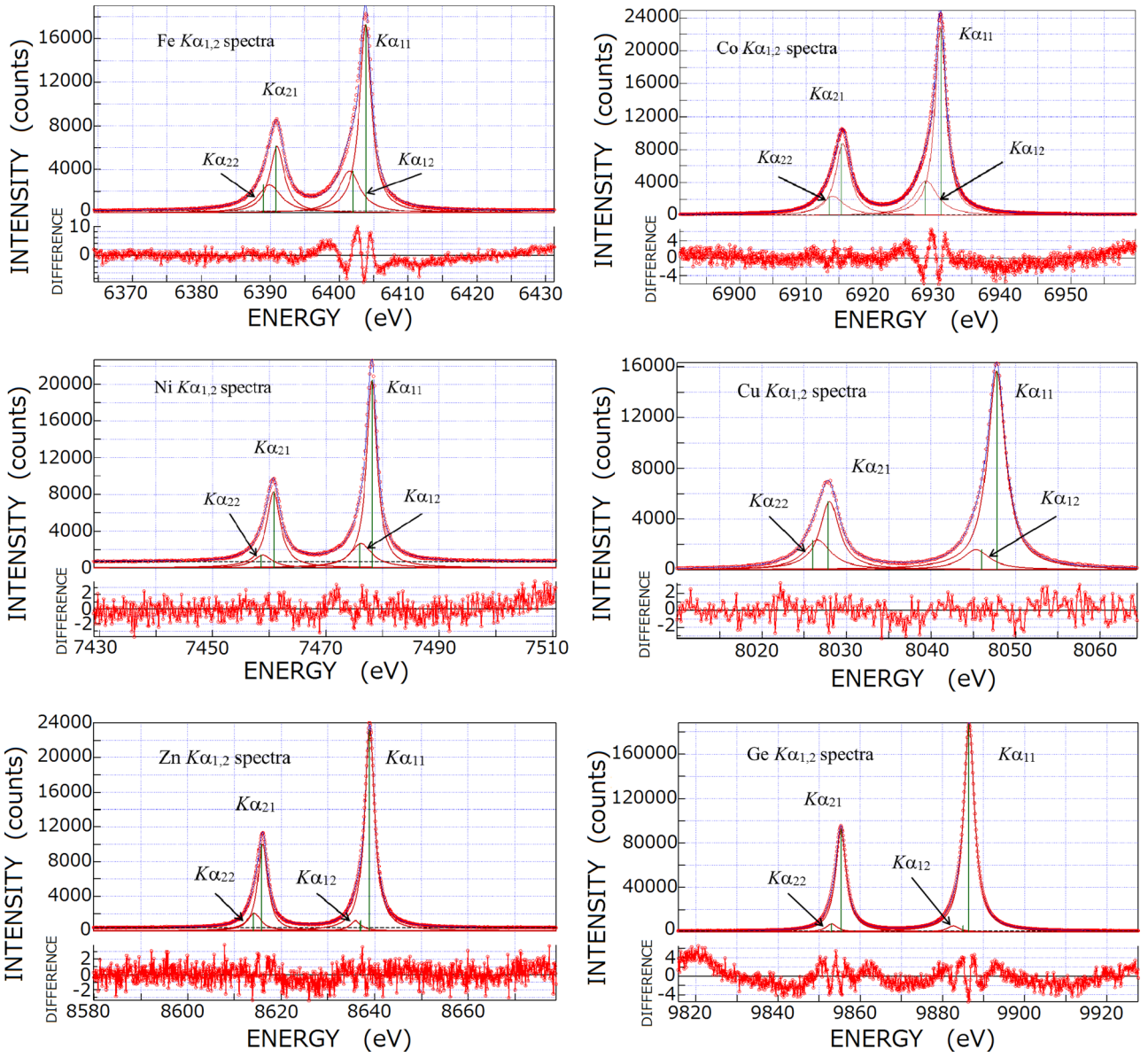

FIG. 3. The observed $K\alpha_{1,2}$ spectra in elements Fe to Ge are shown with the Lorentzian functions used in the fitting process [6,9,11]. These spectra were measured using the antiparallel double-crystal x-ray spectrometer described in the text. $K\alpha_{11}$ is the $K\alpha_1$ diagram line, and $K\alpha_{21}$ is the $K\alpha_2$ line. $K\alpha_{12}$ and $K\alpha_{22}$ satellite lines are due to $2p \rightarrow 1s$ electron transitions in the presence of an extra $3d$ hole resulting from shake processes.

For example, in the case of Ti and Ge the shake-off plus shake-up probabilities for removing an electron from the $3d_{3/2}$ or $3d_{5/2}$ orbitals $[Q_K(3d_{3/2,5/2})]$ the intensity of each satellite line relative to the correspondent diagram line $I_D(K\alpha_{1,2})$ is given by the Oohashi approach [54],

$$\frac{I_S(K\alpha_{1,2})}{I_D(K\alpha_{1,2})} = \frac{Q_K(3d_{3/2,5/2})\frac{\Gamma^+_{K\alpha_{1,2}}}{\Gamma^+_{K_{tot}}}}{[1-Q_K(3d_{3/2,5/2})]\frac{\Gamma_{K\alpha_{1,2}}}{\Gamma_{K_{tot}}}}, \quad (3)$$

where $K\alpha_{1,2}$ and $\Gamma_{K_{tot}}$ denote radiative and total level widths, respectively, with the same meaning as above for the sign "+", and K refers to orbital $1s$.

IV. RESULTS AND DISCUSSION

A. The observed $K\alpha_{1,2}$ emission spectra

The $K\alpha_{1,2}$ spectra of elements Ca to Ge have been measured several times with a high-resolution double-crystal x-ray spectrometer. The FWHM of the $K\alpha_{11}$ and $K\alpha_{21}$ diagram lines, corrected for the instrumental broadening, are presented in Figs. 4(a) and 4(b), together with the recommended values based on experimental results of Campbell and Papp [55]. The values of the obtained averaged line energies, averaged FWHM, averaged asymmetry indexes, averaged relative intensity ratios for each line in the asymmetric model, averaged line energies, averaged observed FWHM, averaged corrected FWHM (CF), and averaged relative intensity ratio in each Lorentzian model, for Ca, Sc, Ti, Cr, Mn, Fe, Co, Ni, and Ge,

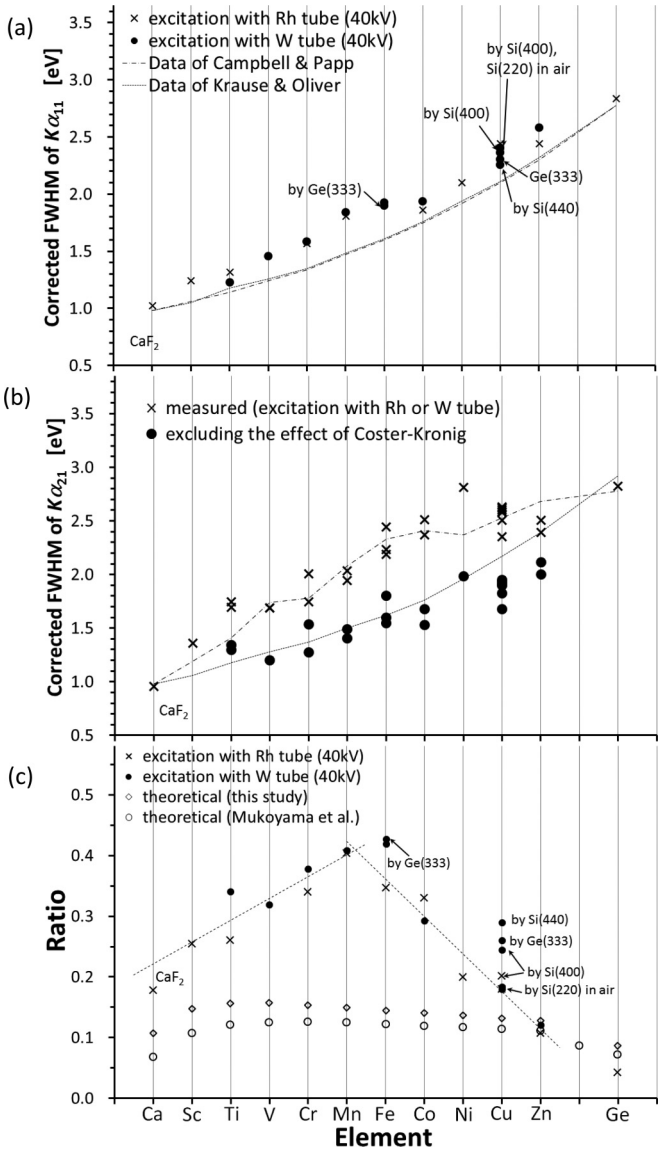

FIG. 4. (a) The corrected FWHM (CF) of the $K\alpha_{11}$ line of elements Ca to Ge together with the semiempirical values reported by Krause and Oliver [13], and recommended values of Campbell and Papp [55]. The widths of Krause and Oliver are semiempirical values and those reported by Campbell and Papp are recommended values based on experimental results. (b) The CF of the $K\alpha_{21}$ line of elements Ca to Ge is shown together with the recommended values [55]. Open circles and thick crosses are the values subtracting the Coster-Kronig broadening effects reported by Nyholm *et al.* [56]. The CF values for both the $K\alpha_{11}$ and $K\alpha_{21}$ diagram lines were obtained from the observed FWHM through Tochio's method [17]. (c) Ratio of satellite to diagram line intensities for elements Ca to Ge, compared with our theoretical values and those of Ref. [57].

are shown in Table II, as well as the semiempirical natural linewidths [13], and Campbell and Papp's recommended linewidth values [55]. The Lorentzian model was used for an analytic representation of each $K\alpha$ line [6,9,11], and the fitting Lorentzian functions are shown in Figs. 2 and 3. The errors quoted in Table II are thus only statistical errors resulting from the fitting processes, and the limited reproducibility of the experimental setup. To obtain realistic uncertainties, the errors originating from the energy calibration have to be considered. Absolute $K\alpha_{1,2}$ and $K\beta_{1,3}$ photon energies for all $3d$ elements between Cr and Cu can be found in Ref. [7].

Several attempts hitherto have been made to obtain a physical interpretation of the observed Z dependence of the lines characteristic parameters, such as the width, asymmetry index, etc., over a wide Z range. A well-known identification of the line shape is generally based on its FWHM and its asymmetry index. Both values allow for a comparison with other experimental results and a general classification of our measurements relative to other reference data. However, it should be noted that the line shape cannot be described precisely by a simple asymmetric profile in all cases, including the $K\alpha$ lines, as also suggested by Höltzer *et al.* [7]. Moreover, it is noteworthy that various width values from previous measurements on $3d$ elements do not include complete corrections for the instrumental broadening [7]. The advantage of the double-crystal spectrometer setup lies in the fact that the "true" FWHM of the emission line can be determined by a simple subtraction of the crystal dispersion from the FWHM of the measured emission line [17]. This approach was employed in this work.

In Figs. 4(a) and 4(b) we can see that the overall variation behavior with Z of the corrected FWHM of the $K\alpha_{11}$ and $K\alpha_{21}$ lines as a function of Z is well reproduced by the data reported by Campbell and Papp [55] but the latter, except for Ca and Ge, are systematically smaller than the present values by about 20%. We obtained the CF values for both $K\alpha_{11}$ and $K\alpha_{21}$ diagram lines from the observed FWHM through Tochio's method [17]. As seen in Fig. 4(b), the CF values of the $K\alpha_{21}$ lines are well consistent with those of the $K\alpha_2$ from CP [55], and are about 0.5 eV larger than those of the $K\alpha_2$ lines from KO [13]. For Zn, they are almost the same as the calculated values reported in Figs. 4(a) and 4(b). From the difference of CF values in $K\alpha_{11}$ and $K\alpha_{21}$ diagram lines, we can conclude that the L_2-$L_3M_{4,5}$ Coster-Kronig transitions begin around Sc ($Z = 21$) and disappear around Zn ($Z = 30$), as seen in Fig. 4(b). This is also seen in this figure if we take into account the Coster-Kronig broadening effects reported by Nyholm *et al.* [56]. It is found that the FWHM values of the $K\alpha_{21}$ lines, excluding the broadening effects, are consistent with the FWHM of $K\alpha_2$ lines from KO [13].

As seen in the analysis of the $K\alpha_{1,2}$ spectra of Figs. 2 and 3, the increase in FWHM of the $K\alpha_1$ and $K\alpha_2$ diagram lines may be related to the contribution of the shake processes. According to the shake process theory, when K-shell ionization is accompanied by additional outer shell ionization or excitation, as often happens, the subsequent $K\alpha$ x-ray peaks are shifted in energy relative to the diagram lines. For instance, the simultaneous ionization in the K and L shell leads to $K\alpha_{12}$ and $K\alpha_{22}$ satellite lines, easily resolved from the diagram lines using an x-ray crystal spectrometer. However, when ionization occurs in K and M or N shells, the $K\alpha$ satellite energy shift is generally less than the natural linewidth of the diagram lines. Therefore, the diagram lines, especially in $3d$ and $4s$ elements, can be strongly contaminated by these so-called hidden satellites.

Two Lorentzian shapes for each diagram line were applied for the systematic analysis of those elements. $K\alpha_{12}$ and $K\alpha_{22}$

TABLE II. The averaged fitting parameters for the $K\alpha_{1,2}$ spectra using four or five symmetric and two asymmetric Lorentzians. A four- or five-Lorentzian functions fitting is used for the contribution of the shake processes and obtaining the natural linewidths. The energy, the FWHM, and the corrected FWHM (CF) are in eV, NIR stands for the normalized intensity ratio, AI stands for asymmetric index, and KO and CP stand for corrected FWHM from Krause and Oliver [13], and Campbell and Papp [55], respectively. Uncertainties are indicated within parentheses. All specimens are metallic, except for Ca. In this case a CaF_2 specimen was used. For all presented cases the primary target was Rh and the spectrometer crystal was Si(220)×2.

Line	Energy	FWHM	CF	KO	CP	NIR	Line	Energy	FWHM	AI	NIR
Ca	Five sym. fitt.						Two asym. fitt.				
$K\alpha_{11}$	3691.687(35)	1.079(6)	1.023(6)	0.98	0.98	100	$K\alpha_1$	3691.631(35)	1.229(4)	0.771(2)	100
$K\alpha_{12}$	3692.682(45)	2.09(24)				14.3(3.6)					
$K\alpha_{21}$	3688.101(35)	1.015(9)	0.957(9)	0.98	0.98	46.83(79)	$K\alpha_2$	3688.105(37)	1.235(3)	0.827(6)	49.96(13)
$K\alpha_{22}$	3688.849(17)	1.743(57)				10.1(1.1)					
$K\alpha''$	3694.536(38)	2.43(12)				7.1(1.0)					
Sc	Five sym. fitt.						Two asym. fitt.				
$K\alpha_{11}$	4090.592(12)	1.309(15)	1.243(15)	1.05	1.06	100	$K\alpha_1$	4090.565(13)	1.635(7)	1.060(14)	100
$K\alpha_{12}$	4089.38(14)	2.291(81)				16.1(1.7)					
$K\alpha_{21}$	4085.765(18)	1.421(49)	1.358(49)	1.06	1.19	42.3(4.6)	$K\alpha_2$	4085.770(16)	1.889(11)	0.869(8)	52.55(39)
$K\alpha_{22}$	4086.29(19)	3.66(57)				25.2(2.7)					
$K\alpha''$	4093.484(19)	1.742(31)				5.83(0.18)					
Ti	Five sym. fitt.						Two asym. fitt.				
$K\alpha_{11}$	4510.832(13)	1.393(8)	1.319(8)	1.16	1.14	100	$K\alpha_1$	4510.832(16)	1.821(1)	1.224(2)	100
$K\alpha_{12}$	4509.604(55)	2.78(10)				25.39(20)					
$K\alpha_{21}$	4504.701(14)	1.757(29)	1.693(29)	1.18	1.41	49.7(2.5)	$K\alpha_2$	4504.692(15)	2.270(9)	0.851(2)	52.85(22)
$K\alpha_{22}$	4505.66(23)	5.12(36)				25.27(68)					
$K\alpha''$	4514.029(16)	1.538(24)				3.364(74)					
Cr	Four sym. fitt.						Two asym. fitt.				
$K\alpha_{11}$	5414.682(20)	1.657(12)	1.565(12)	1.35	1.34	100	$K\alpha_1$	5414.759(26)	2.298(8)	1.572(9)	100
$K\alpha_{12}$	5412.980(75)	4.543(69)				45.4(2.7)					
$K\alpha_{21}$	5405.490(36)	2.090(34)	2.007(34)	1.37	1.78	47.2(2.3)	$K\alpha_2$	5405.417(36)	2.720(21)	0.911(3)	50.09(40)
$K\alpha_{22}$	5405.317(55)	5.97(38)				30.5(1.2)					
Mn	Five sym. fitt.						Two asym. fitt.				
$K\alpha_{11}$	5898.731(61)	1.902(15)	1.806(15)	1.48	1.47	100	$K\alpha_1$	5898.841(62)	2.783(8)	1.712(11)	100
$K\alpha_{12}$	5896.707(70)	4.231(68)				48.5(1.6)					
$K\alpha_{21}$	5887.851(66)	2.125(87)	2.033(87)	1.50	2.08	34.75(4.0)	$K\alpha_2$	5887.702(65)	2.909(11)	1.122(12)	47.55(24)
$K\alpha_{22}$	5887.167(90)	4.37(23)				42.7(4.0)					
Fe	Five sym. fitt.						Two asym. fitt.				
$K\alpha_{11}$	6403.782(71)	2.012(30)	1.912(30)	1.61	1.60	100	$K\alpha_1$	6403.859(71)	2.955(9)	1.693(6)	100
$K\alpha_{12}$	6401.627(99)	3.871(67)				47.8(3.3)					
$K\alpha_{21}$	6390.939(97)	2.54(11)	2.45(11)	1.62	2.33	46.6(5.8)	$K\alpha_2$	6390.765(74)	3.031(10)	1.182(12)	47.559(229)
$K\alpha_{22}$	6389.73(25)	4.123(63)				29.897					
Co	Four sym. fitt.						Two asym. fitt.				
$K\alpha_{11}$	6930.267(57)	1.980(23)	1.857(23)	1.76	1.75	100	$K\alpha_1$	6930.341(60)	2.766(5)	1.549(8)	100
$K\alpha_{12}$	6928.220(56)	4.200(46)				41.2(2.0)					
$K\alpha_{21}$	6915.417(68)	2.487(32)	2.373(32)	1.76	2.41	44.5(1.6)	$K\alpha_2$	6915.317(73)	3.116(11)	1.280(21)	49.82(24)
$K\alpha_{22}$	6914.15(11)	4.473(52)				29.96(70)					
Ni	Four sym. fitt.						Two asym. fitt.				
$K\alpha_{11}$	7478.148(65)	2.229(23)	2.101(23)	1.94	1.92	100	$K\alpha_1$	7478.190(66)	2.744(16)	1.299(5)	100
$K\alpha_{12}$	7476.21(11)	4.57(12)				25.9(2.4)					
$K\alpha_{21}$	7460.807(78)	2.934(22)	2.817(22)	1.96	2.37	53.0(1.6)	$K\alpha_2$	7460.751(86)	3.298(13)	1.176(7)	51.40(21)
$K\alpha_{22}$	7459.0(18)	4.04(13)				12.09(82)					
Ge	Four sym. fitt.						Two asym. fitt.				
$K\alpha_{11}$	9886.47(10)	3.024(10)	2.840(10)	2.78	2.78	100	$K\alpha_1$	9886.50(10)	3.165(7)	1.069(6)	100
$K\alpha_{12}$	9882.68(25)	3.68(23)				3.39(40)					
$K\alpha_{21}$	9855.32(12)	3.008(19)	2.824(19)	2.92	2.78	50.54(32)	$K\alpha_2$	9855.30(12)	3.169(12)	1.077(15)	51.84(13)
$K\alpha_{22}$	9852.73(25)	3.26(27)				3.18(55)					

lines are attributed to the $[KM]$ shake contribution. The calculated transition probability values after $[KM]$ double excitation are shown in Fig. 4(c) together with the observed relative intensity of $K\alpha_{12}$ and $K\alpha_{22}$ lines, and the transition

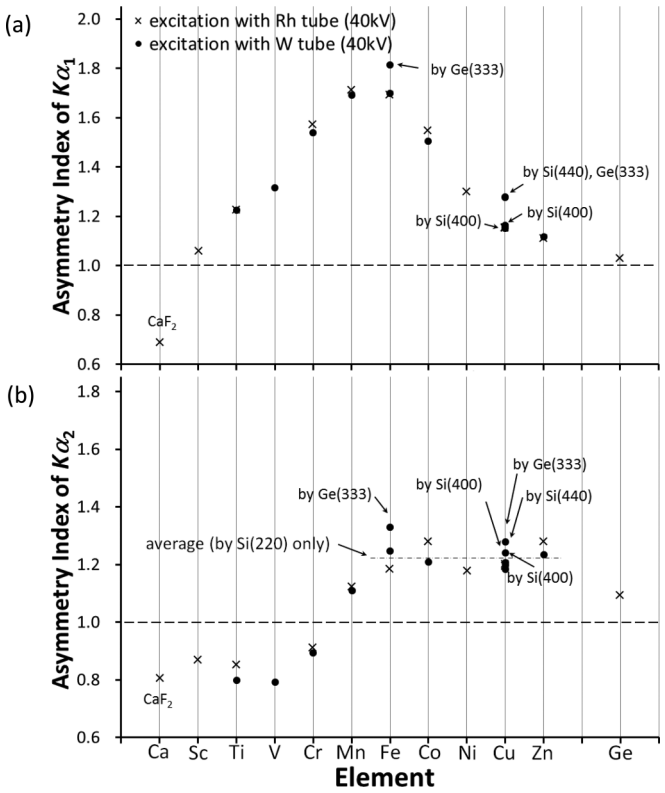

FIG. 5. Values of the asymmetry index of the $K\alpha_1$ and $K\alpha_2$ lines in elements Ca to Ge are shown in (a) and (b), respectively (see text for details).

probability reported by Mukoyama and Taniguchi [57]. We estimated the $[KM]$ shake probability, not including the $3s$ subshell, using the $(K\alpha_{12} + K\alpha_{22})/(K\alpha_{11} + K\alpha_{12} + K\alpha_{21} + K\alpha_{22})$ intensity ratio for Cr to Ge, and the $(K\alpha_{12} + K\alpha_{22} + K\alpha'')/(K\alpha_{11} + K\alpha_{12} + K\alpha_{21} + K\alpha_{22} + K\alpha'')$ intensity ratio for Ca to V. The calculated $[KM]$ shake probabilities increase almost linearly with atomic number, as shown in Fig. 4(c). However, the observed shake probability has a maximum around Mn. The asymmetry index value also has a maximum around this element, as seen in Fig. 5. Owing to the transition of an electron from the complete $2p$ subshell to the $1s$ subshell by the $K\alpha$ emission, the final state has one vacancy in the $2p$ subshell. Besides, the exchange interaction between the electrons of the incomplete $3d$ subshell of transition elements and those of the incomplete $2p$ subshell in the final state may be taken in account, as suggested by Tsutsumi and Nakamori [58], a M_2-$M_3M_{4,5}$ super Coster-Kronig transition should also be considered in the transition elements. More recently, Lowe *et al.* [15] pointed out that these deviations were ascribed to the unique electronic structure of the atoms in the elements with a fully populated $4s$ and an open $3d$ subshell, leading to excitation dynamics in the x-ray emission process. In particular, the number of unpaired electrons is maximal for Mn, which corresponds well to the experimentally observed maximum in the satellite intensity [see Fig. 4(c)].

Moreover, it is noteworthy that the shake probability in these elements has almost the same value when both W and Rh targets are used as an excitation origin.

B. Comparison of experimental data with theoretical calculations based on the shake processes in Ti, Ca, and Ge

The AI values of $K\alpha_1$ and $K\alpha_2$ lines in these elements are shown in Figs. 5(a) and 5(b), respectively. It is noteworthy that in Ge, the $K\alpha_1$ and $K\alpha_2$ spectra profiles are symmetric, as seen in Figs. 5(a) and 5(b), and in Ca the AI value is lower than 1.0, which means that, for each diagram line, the satellite lines, mainly attributed to the $[1s3p]$ shake processes, are on the higher energy side, as seen in Figs. 2 and 3. However, in Sc the AI value is almost 1.0 but the satellite line resulting from the $[1s3d]$ shake process lies on the low-energy side of the $K\alpha_1$ emission line. As the $K\alpha''$ satellite, due to the $[1s3p]$ shake, is on the high-energy side of the $K\alpha_1$, the profile of the $K\alpha_1$ spectrum appears to be symmetric.

For Ti, Chantler *et al.* [16] reported that the observed $K\alpha_1$ spectra had symmetric profiles in disagreement with the results of the Cu $K\alpha_{1,2}$ spectra reported by Deutsch *et al.* [6]. However, although we measured the Ti $K\alpha_{1,2}$ spectra several times using double Si(220) crystals and two kinds of the primary targets, Rh and W, we could not confirm the symmetry of the Ti $K\alpha_1$ emission line. We found the AI value shown in Fig. 5.

The shapes of the theoretically predicted spectra for Ti, Ca, and Ge, obtained as a superposition of different contributions corresponding to diagram and various satellite lines (the latter resulting from the creation of particular outer-shell holes), are compared with the experimental spectra in Fig. 6. The relative intensities for the satellite lines (i.e., peak areas) have been evaluated taking into account the results of the shake-off and shake-up probabilities for the given outer-shell electrons.

According to the theoretical calculation, a contribution from $3d$ electron satellite lines in Ti clearly exists between the $K\alpha_{11}$ and $K\alpha_{21}$ lines, as seen in Fig. 6(a). This corresponds to the position of the observed lines resulting from shake processes, namely, the $K\alpha_{22}$ line, in Ti $K\alpha_{1,2}$ spectra (Fig. 2). In Fig. 6(a) the Ti $K\alpha_{1,2}$ theoretical synthesized spectrum is presented, including diagram and mainly $3d$ satellite lines. Moreover, we evaluated theoretically the contribution of the $3d$ electrons to the diagram lines in the Ti $K\alpha$ emission lines, because it is very difficult to obtain experimentally only the $3d$ electron shake probability contribution in Ti ($3d^2$). Using Eq. (1) we obtained $Q_K(3d) = 9.4463 \times 10^{-2}$, resulting from averaging (with standard deviation of 0.007 34) the overlap integral result for all $3d$ levels. With this value in Eq. (3) we got $I_S(K\alpha_{1,2})/I_D(K\alpha_{1,2}) = 0.0671$.

From the fitted $K\alpha_{1,2}$ spectra we see (Figs. 2 and 3) that as Z decreases, the $K\alpha_{22}$ line crosses over the $K\alpha_{21}$ line in Mn, and in Ca, with no $3d$ electrons, only the $[1s3p]$ shake satellite line seems to appear in the $K\alpha_{1,2}$ spectrum of this element. The theoretical calculation of the Ca $K\alpha_{1,2}$ spectrum, including the contribution from the shake process, agrees with the observed emission lines as seen in Fig. 6(b). In Ge, the shift in $K\alpha_{12}$ x-ray energy due to the $[1s3d]$ transitions is smaller than the natural width of the diagram lines, as seen in Fig. 6(c). Therefore, the small contribution from the satellite line ascribed to the $[1s3d]$ shake processes is reflected in the asymmetry index, as seen in Figs. 5(a) and 5(b). The simulations of the effective spectral shapes predicted theoretically as combinations of different

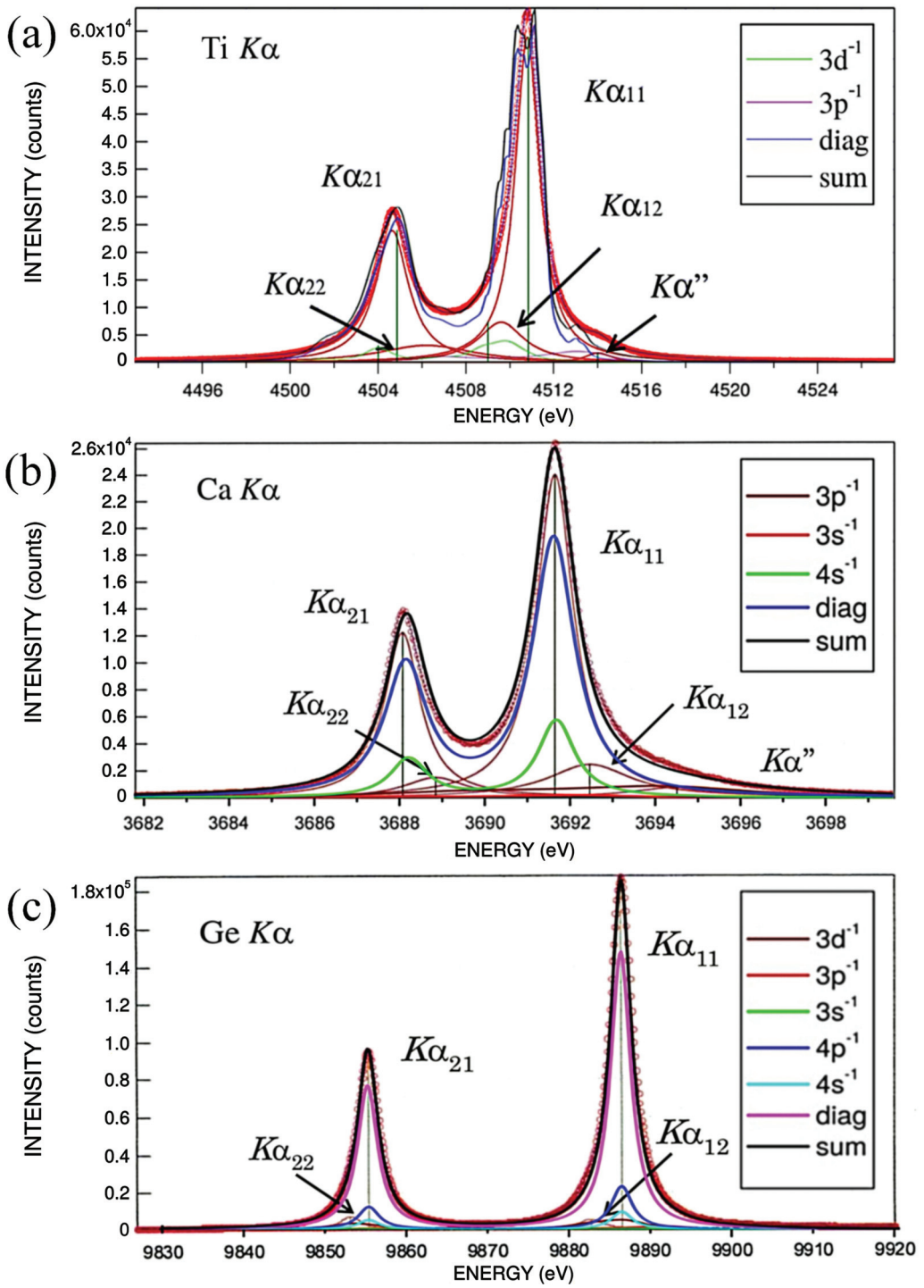

FIG. 6. The calculated $K\alpha_{1,2}$ spectra of Ti, Ca, and Ge are shown in (a) for Ti, (b) for Ca, and (c) for Ge, respectively, together with the observed ones. The spectra include the contributions of the $K\alpha_1$ and $K\alpha_2$ diagram lines, and the satellite lines (in different colors, identified in the legend) predicted on the basis of the shake processes probabilities, $[1s3d]$ and $[1s3p]$ for Ti, $[1s3p]$, $[1s3s]$, and $[1s4s]$ for Ca, and $[1s3d]$, $[1s3p]$, $[1s3s]$, $[1s4p]$, and $[1s4s]$ for Ge, respectively. The Lorentzian functions used in the fitting process are also identified, as in Figs. 2 and 3.

contributions corresponding to diagram and various satellite lines have been obtained by using probabilities of shake processes for various M and N subshells. As seen for Ca and Ge in Figs. 6(b) and 6(c), our theoretical predictions reproduce very well the high-resolution experimental emission data. Also in the case of open shell Ti our theoretically predicted synthetic spectrum is in good agreement with the experimental one [see Fig. 6(a)].

V. CONCLUSIONS

We measured and analyzed systematically the $K\alpha_{1,2}$ diagram lines in elements Ca to Ge, using a double-crystal x-ray spectrometer, considering from the theoretical point of view the electronic transitions.

The natural linewidths, asymmetry indexes, and $[KM]$ shake probabilities in elements Ca to Ge are investigated from the measurement of the $K\alpha_{1,2}$ diagram lines. The averaged corrected FWHM values of the $K\alpha_1$ emission line in these elements are very consistent with the recommended and semiempirical ones. However, those of the $K\alpha_2$ line become large relative to the FWHM values above Mn, but are consistent with the recommended ones. It is found that the anomaly in the $K\alpha_2$ line is ascribed to the Coster-Kronig broadening effects.

The asymmetry index in the $K\alpha_1$ spectral profile is larger than 1.0 from Ti until Zn. Although in Sc the satellite transition resulting from the $[1s3d]$ shake lies in the low-energy side of the $K\alpha_1$ emission line, this line shows a symmetric profile due to the contribution of the $K\alpha''$ satellite line (resulting from the $[1s3p]$ shake).

Although the asymmetry index of the $K\alpha_2$ line profile does not show a clear behavior as Z changes, it has almost constant value between elements Fe and Zn. Moreover, it follows that the asymmetry of $K\alpha_{1,2}$ spectra from Sc to Ge is mainly ascribed to the $[1s3d]$ shake processes.

In elements Ca and Sc, unlike the results reported by Lowe *et al.*, the shake processes contribution to the diagram lines is less than 40%, corresponding to theoretical ones reported by Mukoyama and Taniguchi [57], and in this work, of around 20%. In Ge, the shake probability is almost consistent with that in the theoretical one.

Finally, we believe that the information on the $K\alpha_{1,2}$ spectra obtained in this study is useful for the theoretical calculations concerning the electron correlation in the atom and to the excitation dynamics in the $3d$ transition elements. We also believe that our results will be helpful in the detailed study of line shapes and line energies for $K\alpha_2$ x-ray emission spectra of $3d$ metal atoms in a variety of compounds, as very recently published for Mn compounds [59].

ACKNOWLEDGMENTS

Y.I. acknowledges financial support for the measurements of a part of the data by the REXDAB collaboration that was initiated within the International Fundamental Parameter Initiative. This work is supported also in part by the Polish National Science Center under Grant No. 2011/01/D/ST2/01286. This work was funded partly by Portuguese Foundation for Science and Technology (FCT) under projects UID/MULTI/04046/2013 (BioISI) and UID/FIS/04559/2013 (LIBPhys). Laboratoire Kastler Brossel is Unité Mixte de Recherche de l'UPMC-Sorbonne Universités, du CNRS, de l'ENS-PSL Research University et du Collège de France, No. 8552.

[1] S. K. Allison, Phys. Rev. **44**, 63 (1933); L. G. Parratt, *ibid.* **49**, 502 (1936); H. P. Rosner and C. P. Bhalla, Z. Phys. **231**, 347 (1970); S. I. Salem and R. J. Wimmer, Phys. Rev. A **2**, 1121 (1970); J. H. McCrary, L. V. Singman, L. H. Ziegler, L. D. Looney, C. M. Edmonds, and Carolyn E. Harris, *ibid.* **4**, 1745 (1971); P. L. Lee and S. I. Salem, *ibid.* **10**, 2027 (1974).

[2] P. L. Lee and S. I. Salem, Z. Phys. **43**, 707 (1927).

[3] P. L. Lee and S. I. Salem, J. Phys. C **3**, 285 (1970).

[4] *X-ray Spectra and Electronic Structure of Matter*, edited by A. Faessler and G. Wiech (Fotodruck Frank OHG, Munchen, 1973).

[5] J. Finster, G. Leonhardt, and A. Meisel, J. Phys. Colloq. **32**, C4-218 (1971).

[6] M. Deutsch, G. Hölzer, J. Hartwig, J. Wolf, M. Fritsch, and E. Forster, Phys. Rev. A **51**, 283 (1995).

[7] G. Hölzer, M. Fritsch, M. Deutsch, J. Hartwig, and E. Forster, Phys. Rev. A **56**, 4554 (1997).

[8] C. T. Chantler, M. N. Kinnane, C.-H. Su, and J. A. Kimpton, Phys. Rev. A **73**, 012508 (2006).

[9] H. Berger, X-Ray Spectrom. **15**, 241 (1986).

[10] Y. Ito, T. Tochio, S. Fukushima, A. Taborda, J. M. Sampaio, J. P. Marques, F. Parente, P. Indelicato, and J. P. Santos, J. Quant. Spectrosc. Radiat. Transfer **151**, 295 (2015).

[11] Y. Ito, T. Tochio, H. Oohashi, and A. M. Vlaicu, Radiat. Phys. Chem. **75**, 1534 (2006).

[12] M. Polasik, K. Słabkowska, Y. Ito, J. Rzadkiewicz, T. Tochio, J. Starosta, K. Kozioł, and E. Wiatrowska-Kozioł, Proceedings of the 16th International Conference on Physics of Highly Charged Ions Book of Abstracts B-a16, Heidelberg, Germany, 2012 (unpublished).

[13] M. O. Krause and J. H. Oliver, J. Phys. Chem. Ref. Data **8**, 329 (1979).

[14] D. F. Anagnostopoulos, R. Sharon, D. Gotta, and M. Deutsch, Phys. Rev. A **60**, 2018 (1999).

[15] J. A. Lowe, C. T. Chantler, and I. P. Grant, Phys. Rev. A **83**, 060501(R) (2011).

[16] C. T. Chantler, J. A. Lowe, and I. P. Grant, J. Phys. B **46**, 015002 (2013).

[17] T. Tochio, Y. Ito, and K. Omote, Phys. Rev. A **65**, 042502 (2002).

[18] J. A. Bearden, Rev. Mod. Phys. **39**, 78 (1967).

[19] J. P. Desclaux, Comput. Phys. Commun. **9**, 31 (1975).

[20] I. P. Grant, Int. J. Quantum Chem. **25**, 23 (1984).

[21] P. Indelicato, O. Gorceix, and J. P. Desclaux, J. Phys. B **20**, 651 (1987).

[22] I. P. Grant and H. M. Quiney, Adv. At. Mol. Phys. **23**, 37 (1988).

[23] K. G. Dyall, I. P. Grant, C. T. Johonson, F. A. Parpia, and E. P. Plummer, Comput. Phys. Commun. **55**, 425 (1989).

[24] M. Polasik, Phys. Rev. A **39**, 616 (1989); **39**, 5092 (1989); **40**, 4361 (1989); **41**, 3689 (1990); **52**, 227 (1995); **58**, 1840 (1998).

[25] M. Polasik, K. Słabkowska, J. Rzadkiewicz, K. Kozioł, J. Starosta, E. Wiatrowska-Kozioł, J.-Cl. Dousse, and J. Hoszowska, Phys. Rev. Lett. **107**, 073001 (2011)..

[26] P. Indelicato and J. P. Desclaux, Phys. Rev. A **42**, 5139 (1990).

[27] P. Indelicato, Phys. Rev. A **51**, 1132 (1995).

[28] F. A. Parpia, C. F. Fischer, and I. P. Grant, Comput. Phys. Commun. **94**, 249 (1996).

[29] P. Jönsson, X. He, C. F. Fischer, and I. P. Grant, Comput. Phys. Commun. **177**, 597 (2007).
[30] C. Froese Fischer and G. Gaigalas, Phys. Rev. A **85**, 042501 (2012).
[31] J. P. Santos, J. P. Marques, F. Parente, E. Lindroth, and P. Indelicato, J. Phys. B **32**, 2089 (1999).
[32] M. C. Martins, J. P. Marques, A. M. Costa, J. P. Santos, F. Parente, S. Schlesser, E.-O. Le Bigot, and P. Indelicato, Phys. Rev. A **80**, 032501 (2009).
[33] J. P. Santos, G. C. Rodrigues, J. P. Marques, F. Parente, and P. Indelicato, Eur. Phys. J. D **37**, 201 (2006).
[34] G. Audi, A. H. Wapstra, and C. Thibault, Nucl. Phys. A **729**, 337 (2003).
[35] I. Angeli, At. Data Nucl. Data Tables **87**, 185 (2004).
[36] P. J. Mohr and Y. K. Kim, Phys. Rev. A **45**, 2727 (1992).
[37] P. J. Mohr, Phys. Rev. A **46**, 4421 (1992).
[38] E. O. Le Bigot, P. Indelicato, and P. J. Mohr, Phys. Rev. A **64**, 052508 (2001).
[39] P. Indelicato and P. J. Mohr, Phys. Rev. A **46**, 172 (1992).
[40] P. J. Mohr and G. Soff, Phys. Rev. Lett. **70**, 158 (1993).
[41] P. Indelicato, S. Boucard, and E. Lindroth, Eur. Phys. J. D **3**, 29 (1998).
[42] P. Indelicato and P. Mohr, Hyperfine Interact. **114**, 147 (1998).
[43] P. O. Löwdin, Phys. Rev. **97**, 1474 (1955).
[44] W. R. Johnson, *Atomic Structure Theory: Lectures on Atomic Physics* (Springer, New York, 2010).
[45] R. D. Deslattes, Ernest G. Kessler, Jr., P. Indelicato, L. de Billy, E. Lindroth, and J. Anton, Rev. Mod. Phys. **75**, 35 (2003).
[46] T. A. Carlson and J. C. W. Nestor, Phys. Rev. A **8**, 2887 (1973).
[47] T. A. Carlson, Phys. Rev. **156**, 142 (1967).
[48] T. A. Carlson, C. W. Nestor, Jr., T. C. Tucker, and F. B. Malik, Phys. Rev. **169**, 27 (1968).
[49] M. O. Krause and T. A. Carlson, Phys. Rev. **158**, 18 (1967).
[50] V. P. Sachenko and E. V. Burtsev, Bull. Acad. Sci. USSR, Phys. Ser. **31**, 980 (1968).
[51] J. P. Santos, M. F. Laranjeira, and F. Parente, Europhys. Lett. **55**, 479 (2001).
[52] O. Mauron, J.-Cl. Dousse, S. Baechler, M. Berset, Y.-P. Maillard, P.-A. Raboud, and J. Hoszowska, Phys. Rev. A **67**, 032506 (2003).
[53] O. Mauron, J.-Cl. Dousse, J. Hoszowska, J. P. Marques, F. Parente, and M. Polasik, Phys. Rev. A **62**, 062508 (2000).
[54] H. Oohashi, T. Tochio, Y. Ito, and A. M. Vlaicu, Phys. Rev. A **68**, 032506 (2003).
[55] J. L. Campbell and T. Papp, At. Data Nucl. Data Tables **77**, 1 (2001).
[56] R. Nyholm, N. Måhrtensson, A. Lebuglet, and U. Axelsson, J. Phys. F **11**, 1727 (1981).
[57] T. Mukoyama and K. Taniguchi, Phys. Rev. A **36**, 693 (1987).
[58] K. Tsutsumi and H. Nakamori, J. Phys. Soc. Jpn. **25**, 1418 (1968).
[59] M. Jabua, D. Gotta, T. Strauch, C. Weidemann, B. Fricke, and K. Rashid, Spectrochimica Acta, Part B **121**, 11 (2016).